NEW PARADIGMS FOR BLACK HOLE ACCRETION FROM HIGH RESOLUTION SUPERCOMPUTER EXPERIMENTS

John F. Hawley
Theoretical Astrophysics, Caltech, Pasadena, Ca. 91125

Larry L. Smarr
Astronomy Department, University of Illinois, Urbana, Il. 61801

ABSTRACT

From a series of high resolution supercomputer calculations, new paradigms emerge for black hole accretion with angular momentum. We have discovered that the centrifugal barrier, or funnel wall, plays a key role in shock heating the inflowing supersonic fluid, producing a stationary thick disk with bipolar outflow. The infall dynamics are calculated in detail and followed until a steady state is reached. We delineate a number of distinct regimes of steady state flow in the two parameter solution space defined by the fluid's angular momentum and the disk thickness. The essential physics is highlighted with selected numerical examples. The same code can calculate general relativistic magnetohydrodynamical flows near black holes.

INTRODUCTION

Observations of quasars, active galactic nuclei (AGN), and astrophysical jets have been increasing in number and scope for two decades. The fundamental power source is, in all likelihood, gravitational, with a supermassive black hole providing the potential well (see, e.g., Blandford, this volume). The enormous range in luminosity (10^{39} to 10^{48} ergs s^{-1}) probably reflects a wide variance in accretion rates during the lifetime of a "standard" sized black hole[1] of mass $\approx 10^8 M_\odot$. In addition to this long timescale accretion rate variation, there is growing observational evidence that the accretion process is variable on timescales[2] as short as hours, comparable to the inner orbital periods around such supermassive black holes. Many of the AGN have bulk bipolar flows emerging from them. In certain cases, this outflow forms narrow, highly collimated, supersonic jets.

To date, most theoretical models of black hole disk accretion have been analytic stationary approximations. These yield insight into the time averaged properties of accretion disks, but the highly variable nature of AGN indicates dynamic flows may be necessary to explain the observations.

We have addressed this issue by using a time dependent, fully general relativistic two-dimensional hydrodynamics code which is documented[3,4] in papers I and II. The results in this paper come from a series of high resolution numerical experiments run with this code on the CRAY-1 supercomputer at the Max Planck Institute for Astrophysics in Garching, West Germany. These experiments

0094-243X/86/1440263-28$3.00 Copyright 1986 American Institute of Physics

begin the investigation of realistic dynamic fluid behavior in the gravitational field of a black hole. This paper summarizes some of these new, generic phenomena we have discovered in the near hole region.

SOLVING THE ACCRETION EQUATIONS

In our present study we do not intend to provide detailed astrophysical models of central engines. The physics required to do this would include many complicated effects such as magnetohydrodynamics (MHD), viscosity, radiation hydrodynamics, and relativistic plasma physics. This conference marks an important step toward sorting out the essential physics. We expect that the development of a detailed theory should take at least as long as was required for understanding stellar evolution, where progress was aided by the simplifications of spherical symmetry and a relatively detailed knowledge of nuclear physics. The field of black hole accretion physics is still too immature to hope to obtain such complete models.

We can, as a first step, investigate highly resolved axisymmetric hydrodynamics in near hole regions with the current generation of supercomputers. As additional physics is added in later calculations, fluid dynamical effects will remain, and dominate in some regimes. Our near term goal, therefore, has been to write and use a code which can map out the phenomenology of black hole hydrodynamics solution space. We use time explicit, Eulerian finite differencing to solve the equations of general relativistic ideal hydrodynamics. The particular investigation is of the behavior of fluid with angular momentum in the fixed Kerr black hole metric. In general our results involve phenomena which could not previously be examined, including multiple shock structures, vortical motions and the nonlinear development of instabilities. In addition, the development of carefully tested numerical techniques for hydrodynamics is the requisite first step towards solving the more general and complicated problems involving the MHD equations, viscosity, and radiation transport.

The first attempt to model the behavior of an ideal fluid in a Kerr black hole metric was made by James R. Wilson in 1971 when he studied the axisymmetric infall of cold gas with nonzero angular momentum[5]. This two-dimensional code used cylindrical coordinates and was the predecessor to the present code. During the middle 1970's, Wilson[6-8] added the general relativistic MHD equations to the code. In 1980, this code, including the MHD terms, was rewritten into spherical polar coordinates by Smarr and Wilson.

We have since taken the 1980 hydrodynamics (dropping the MHD terms) code and developed the current production version. Extensive effort has gone into calibration against analytically determined solutions and the comparison of various finite difference techniques. This development involved working out numerous analytic solutions in terms of the code variables and then carrying out hundreds of computer runs to transform the

original 1980 prototype version into an accurate astrophysical research tool. This work is detailed in references 3, 4, 9, and 10.

We briefly remark on the resources necessary to carry out this work. Although much of the calibration work was accomplished on a VAX 11/780, the high resolution runs each require several hours of CRAY-1 time. The total project requirements to date have been some 75 Cray hours (roughly two full VAX years). The great advantage of using a supercomputer is illustrated by the fact that the VAX 11/780 runs in Paper II were done with a grid resolution of 40x30 and took 8 hours of compute time for a full evolution. In contrast, the CRAY-1 (some 200 times faster) could run with a grid resolution of 160x160, taking only two hours to reach the same evolutionary time. A comparison of the resolution of VAX and CRAY runs are displayed in reference 9.

Finally, modern computer imaging is essential to be able to probe the gargantuan amount of numerical output from a supercomputer run. The black and white contour line drawings that we are limited to in this paper are completely inadequate to sort out the physics of the resulting flows. Full color images (at least 512x512x8 bits) and image processing techniques are necessary to represent the information contained in the solution at one time level. The amount of number crunching to produce these images from the raw numerical data in a short time also requires a supercomputer. Finally, the dynamics can be understood only with the use of highly time-resolved color image movies of the sort we have shown at this conference. Our work with these essential tools has only been possible because of the fine imaging facilities at the University of Illinois (VIP System) and at the Max Planck Institute for Astrophysics.

We mention the above points to emphasize that the technology and manpower requirements for performing these calculations, let alone solving more complicated equations, such as MHD, are approaching the requirements (and dollar investments) of observational astronomy. The style of this research in other areas of science actually has a long history[11]. We would like to emphasize that in all phases of our project (the numerical techniques, the unravelling of the hydro physics, the code management, and the color imaging), we benefited greatly from the shared experience of our colleagues James Wilson, Karl-Heinz Winkler, and Michael Norman.

Although it is outside the scope of this paper to describe the expanded MHD version of this code, the reader should be aware that Wilson has used the cylindrically symmetric MHD code to extensively investigate black hole magnetospheres [6-8,12,13]. In those papers one will find the generalization of our equations to MHD and a number of rather complex solutions. No new solutions have been calculated with the code since those papers. It remains a future task of some graduate student to carefully calibrate and improve the MHD portion of the code to achieve the standards of rigor which characterizes our non-MHD code described herein. A first step in this direction was an analytic analysis of the

relativistic MHD equations[14] which included a comparison with the elegant work of Thorne and Macdonald[15]. For a recent review of idealized analytic black hole magnetospheres, see papers in this volume by Blandford and by Lovelace.

The hydrodynamic calculations are performed in a fixed black hole gravitational field; for our accretion problems this field is represented by the Kerr metric $g^{\mu\nu}$ expressed in Boyer-Lindquist coordinates[16]. The Kerr metric represents a rotating black hole. The work reported herein uses the simpler special case of a nonrotating Schwarzschild black hole. At large distances the Schwarzschild coordinates become flatspace spherical coordinates. The metric defines the lapse function $\alpha = (-g^{tt})^{-1/2}$, the shift vector $\beta_i = g_{ti}$ and the three-metric $\gamma_{ij} = g_{ij}$. The dynamic matter is described by the ideal fluid stress-energy tensor $T^{\mu\nu} = (\rho + \rho\varepsilon + P)U^\mu U^\nu + Pg^{\mu\nu}$ where ρ is the baryon density, P is the pressure, ε is the specific internal energy, and U^ν is the 4-velocity of the matter. In our work, we assume that the mass in the gas is much less than the mass of the hole. Therefore we can ignore the gravity of the gas. The reader is referred to several introductions to relativistic hydrodynamics[16,17] for background on notation.

Before beginning our discussion we remind the reader of the equations of general relativistic hydrodynamics[3] as they are applied in our code. First there is the equation of baryon conservation

$$\partial_t D + \frac{1}{\sqrt{\gamma}}\,\partial_i\,(\sqrt{\gamma}\,D\,V^i) = 0, \qquad (1)$$

where $D = W\rho$, U^α is the 4-velocity, $V^i = U^i/U^t$ is the transport velocity, γ is the determinant of the 3-metric, and $W = (1 - V_jV^j)^{-1/2}$ is the redshift factor equal to $U^t\alpha$ where α is the lapse function. Momentum conservation is written

$$\partial_t S_j + \frac{1}{\sqrt{\gamma}}\,\partial_i(S_jV^i\sqrt{\gamma}) + \alpha\partial_j P + \frac{1}{2}\,(\partial_j g^{\mu\nu})\,\frac{S_\mu S_\nu}{S^t} = 0, \qquad (2)$$

where $S_\nu = \rho hWU_\nu$, with relativistic enthalpy $h = 1 + \varepsilon + P/\rho$. Finally, we write the equation of energy conservation

$$\partial_t E + \frac{1}{\sqrt{\gamma}}\,\partial_i\,(\sqrt{\gamma}\,V^iE) + P\partial_t W + \frac{P}{\sqrt{\gamma}}\,\partial_i(\sqrt{\gamma}\,V^iW) = 0, \qquad (3)$$

where $E = \rho\varepsilon\,W$. In these equations $j = r, \theta, \phi$; $i = r, \theta$; and μ and $\nu = r, \theta, \phi, t$. The equation of state that we currently use is that for an ideal gas, $P = \rho\varepsilon(\Gamma-1) = \frac{E}{W}(\Gamma-1)$. In this case, the enthalpy reduces to $h = 1 + \Gamma\varepsilon$. For a complete discussion and derivation of these equations, including their Newtonian limit, see Paper I. Our methods for solving these equations, and the calibration tests of our code, are detailed in Paper II.

In this work, we use geometric units in which G = c = M (the black hole mass) = 1. To recover physical c.g.s. units, multiply the geometric value by the appropriate values of G, c, M. For example, the unit distance is

$$r = 1.5 \times 10^{5} \ (M/M_{\odot}) \ \text{cm}, \qquad (4)$$

and the unit time,

$$t = 5 \times 10^{-6} \ (M/M_{\odot}) \ \text{s}, \qquad (5)$$

where $M_{\odot}$ is the mass of the sun. The temperature of the fluid is given by the specific internal energy, ε, in units of c^2. If we assume the fluid's unit mass to be that of a proton, the temperature is

$$T = \varepsilon m_p c^2/k = 10^{13} \varepsilon \ \text{K}. \qquad (6)$$

Therefore, as is standard convention, we measure distance and time in units of M, and specific internal energy as dimensionless units of $c^2 = 1$. For a complete discussion of geometric units, see reference 16. For scaling, keep in mind that the two most popular astrophysical black hole masses are 10 $M_{\odot}$ (Cygnus X-1) and 10^8 $M_{\odot}$ (AGN central engine).

FUNNEL HYDRODYNAMICS

There are three forces to consider in a purely hydrodynamic accretion flow: gravitational, centrifugal, and thermal pressure gradient. In a cold Keplerian thin disk[18], gravitational and centrifugal accelerations alone balance in the equatorial plane. As pressure becomes important, the vertical thickness of the disk increases, forming the so-called thick disk (see schematic diagram in Fig. 1). In the stationary thick disk[19], all three forces are everywhere in balance. Our work focuses on the dynamic properties of both thin and thick disks where the forces are not in balance.

The central problem in black hole accretion models is how to convert the gravitational potential energy of infalling matter into energy flowing away from the hole (bulk material flow or electromagnetic radiation). Such a process allows the black hole to be the central engine of an AGN. Much attention has been focused on whether this outflow can be highly collimated into a narrow jet in the near hole region and shot out along the orbital axis. A key feature of the thick disk is the funnel (see Fig. 1), a region along the orbital axis kept empty of fluid by centrifugal acceleration. The existence of these funnels has been argued to be an integral part of the jet formation process (see refs. below).

To define the "funnel wall", we must consider the total "effective potential" around the black hole which represents the combined effects of gravity and rotation. This potential is parameterized by the fluid's specific angular momentum

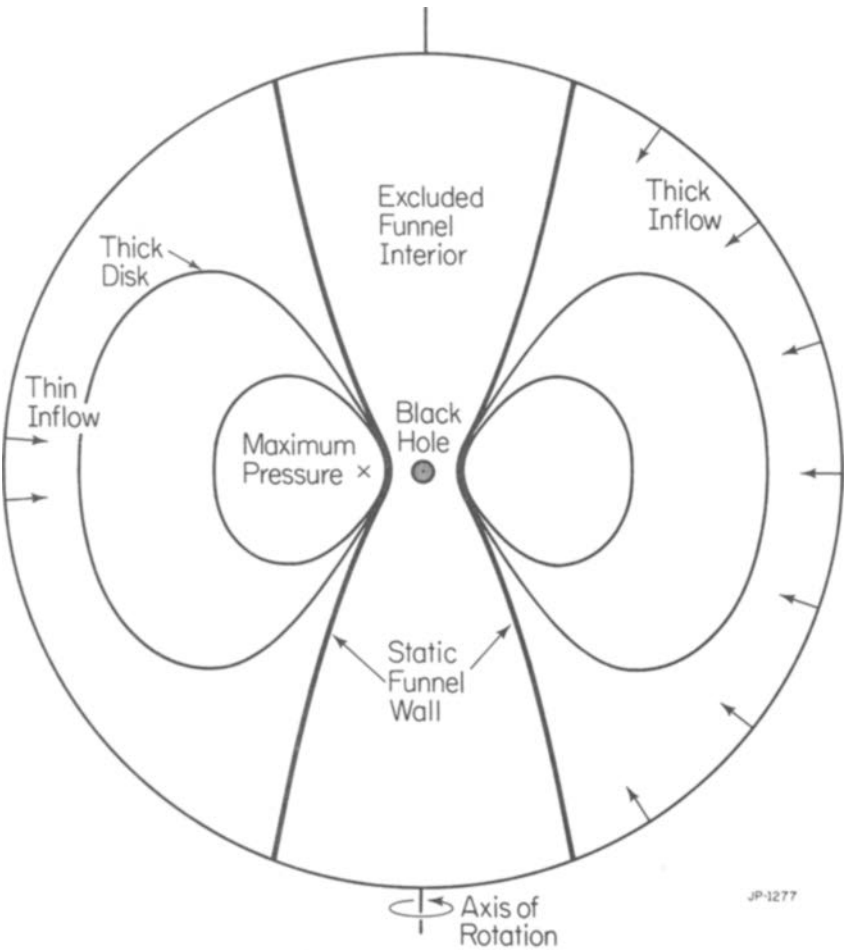


Fig. 1. Schematic diagram of our black hole accretion runs. The outer boundary is r = 100 M. Two major classes of outer boundary conditions are the thick and thin inflows.

$\ell = - U_\phi/U_t$. The effective potential determines the orbit of a test particle with a given value of angular momentum ℓ (see Figure 2). In general relativity, unlike Newtonian gravity, qualitatively different behavior in a test particle's orbit occurs for different ranges of ℓ. There are two critical values of ℓ which divide the possible orbits into three types[19,20]. We will confine the present discussion to the nonrotating Schwarzschild black hole; generalizations to the Kerr black hole are in the literature.

The first critical angular momentum is the "marginally stable" value $\ell_{ms} = 2\sqrt{3}\ M \simeq 3.46\ M$, which is the angular momentum

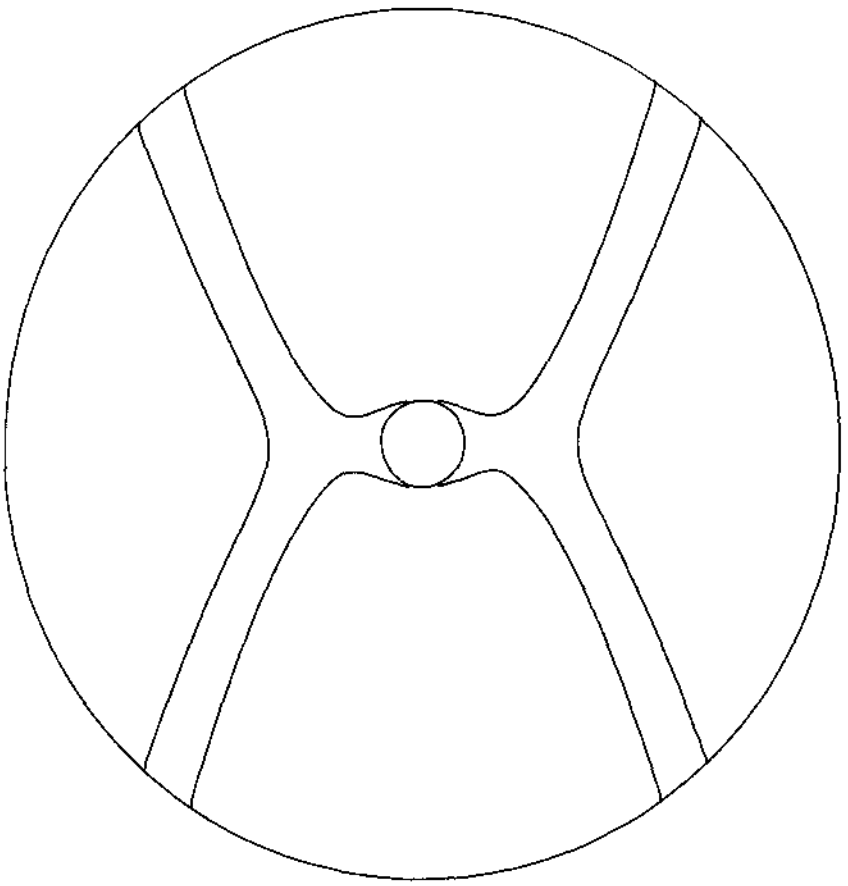


Fig. 2. The effective potential as a function of r along the equator for a Schwarzschild (nonrotating) black hole. From bottom to top the curves are for U_ϕ = 3.0 M, U_ϕ = 2$\sqrt{3}$ M (marginally stable), U_ϕ = 3.8 M, U_ϕ = 4.0 M (marginally bound), and U_ϕ = 4.5 M. Note the important general relativistic effect: the potential does not monotonically increase as r approaches the horizon.

and energy of the closest stable circular orbit around a black hole. This orbit is located at r = 6 M with energy U_t = -0.943. Note that the specific binding energy per unit particle mass of a particle orbit is U_t + 1, in units of c^2. This shows that the marginally stable circular orbit has a binding energy of 0.057 c^2. The other critical value of ℓ is the "marginally bound" value, ℓ = 4.0 M, which is the smallest amount of angular momentum which will keep a particle, falling from rest at infinity (marginally bound orbit with U_t = -1.0), from falling into the hole.

These critical values of ℓ arise[16] from a purely relativistic effect---the "pit in the potential." The relativistic centrifugal effective potential is the generalization of the Newtonian

effective potential, $- M/r + \ell^2/(2r^2)$ (see reference 16, Box 25.6). The relativistic potential has a maximum in the black hole geometry, whereas the corresponding Newtonian potential for a point mass goes to infinity as $r \to 0$. If $\ell < \ell_{mb}$ then this potential maximum drops below the energy ($U_t = -1.0$) where it can provide a turning point for a marginally bound orbit. If $\ell < \ell_{ms}$ the potential curve ceases to have a minimum and no circular orbit is possible (Fig. 2). Neither of these effects can occur in Newtonian gravity, thus providing new modes of accretion specific to black holes.

This one-dimensional analysis has been extended off the equatorial plane to determine the two-dimensional locus of turning points for a marginally bound test particle with a given angular momentum[19-22]. This locus is termed the "funnel wall"; by definition, the test particle is excluded from the interior of this wall. Two qualitatively different topologies of funnel walls result (see Fig. 3). For $\ell > \ell_{mb}$, the funnel wall crosses the equator and no inflow into the hole from any angle can occur. As ℓ decreases below ℓ_{mb}, the wall opens around the equator allowing some fluid to flow into the hole. Thus ℓ provides a crucial parameter describing fluid behavior.

This description of the funnel wall derives from a consideration of the dynamics of test particles, i.e., pressureless, noninteracting gas. One of the goals of our investigation is to determine whether this paradigm of the test particle funnel applies to the more realistic case of gas with pressure. How does the funnel affect such flows and what are its implications for jet production and disk formation?

Lynden-Bell[23] described the funnels in the context of jets, noting that their geometry was ideal for the production of a bi-directional flow inside the evacuated funnel interior. One speculative model, explored by many investigators[24-26], requires the coupling of electromagnetic radiation effects to the hydrodynamics. This model envisions that the intense electromagnetic radiation in the funnels of a thick disk accelerates relativistic plasma out along the orbital axis, i.e., the interior of the funnel. The accretion disk is radiation supported with a surface luminosity on the order of 10^{46} $(M/10^8 M_\odot)$ ergs s^{-1}. Given a sufficiently steep funnel wall, provided by the appropriate ad hoc angular momentum distribution in the thick disk, a narrow, relativistic, and highly collimated jet results. Unfortunately, it seems that radiation drag in the funnel prevents jet acceleration to high velocities[27]. In any case, many radio jets are observed to emerge from galaxies with nuclear luminosity much less than 10^{46} ergs s^{-1}, thus ruling out such radiation pressure supported thick disks in these sources[28]. Both of these points raise serious questions about the viability of this particular black hole jet production mechanism.

Rather than adding additional physics, such as radiation in the funnel, our investigation has centered on whether purely hydrodynamical processes can cause outflow of heated material from gas initially inflowing toward the hole. Because the centrifugal

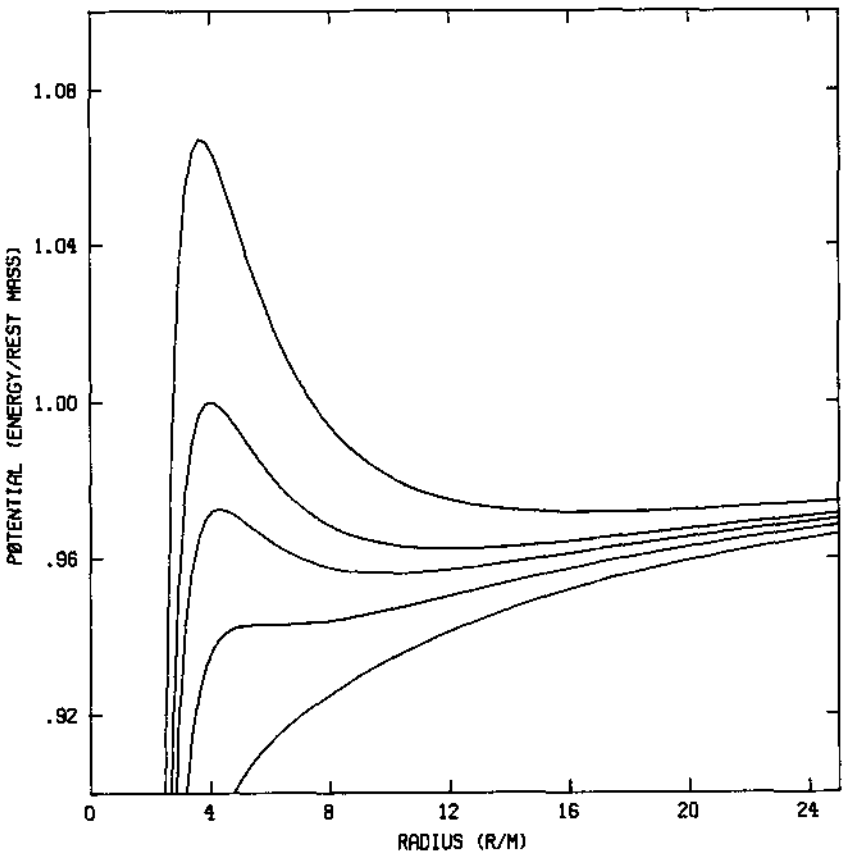


Fig. 3. The funnel walls for ℓ = 3.8 M and ℓ = 4.5 M are depicted. The ℓ = 4.5 funnel wall crosses the equator at r = 7 M.

forces in a hydrodynamic flow will keep the interior of the funnel empty, it has been previously assumed that hydrodynamic infall could not produce jets. The funnel wall was believed to divide the infalling fluid from the vacuum funnel interior. Even if fluid were heated near the hole, it was thought that confinement from the funnel wall and ram pressure from the infalling fluid would prevent the hot fluid's escape.

However, we have discovered that the solution to the full hydrodynamic equations provides a way out of this seeming difficulty. The funnel wall behaves as if it were an actual physical wall and creates a standoff shock. The shocked fluid then flows down towards the equator, hugging the interior of the standoff shock, leaving an evacuated region between the shocked fluid and the funnel wall. The surface of the infalling fluid therefore does not occur at the funnel wall. This creates an escape route out along which hot fluid may jet from the near hole

region. Thus, from these hydrodynamic solutions come new black hole flow paradigms which supplant those based upon test particle notions. These new scenarios are described below.

In our hydrodynamic models, as in the test particle case, we expect qualitatively different behavior depending on whether ℓ is greater or less than ℓ_{mb}. Below we describe several representative cases which highlight the essential physics.

DISK DYNAMICS

Consider first the fate of cold fluid with angular momentum beginning to fall onto a naked hole. This gas may come from cold intragalactic gas surrounding a central black hole. In the standard picture, one assumes that the specific angular momentum is very high, $\ell >> \ell_{mb}$. As it falls towards the hole, it settles down into orbits lying in the equatorial plane at large distance ($r > 100$ M) from the hole. This gas forms a Keplerian thin disk, with a gradual mass flow inward determined by viscous torques. The heating which accompanies these torques is assumed to be promptly radiated away. These assumptions mean that the disk is a steady state fluid.

The total energy radiated over this secular infall timescale is equal to the binding energy of the last stable circular orbit. Because the energy release is gradual, the instantaneous luminosity is lowered. (For a review of thin disks, see Lamb, this volume). If the viscous heating proceeds too rapidly to be promptly radiated, the thin disk is assumed to "puff up" and become a pressure supported thick disk. The interior properties of the thick disk are then determined by viscous and radiation processes.

These standard models represent one extreme of black hole accretion, namely a flow which is dominated by viscosity and initially has high ℓ. Our models study the other extreme: the free dynamical infall of low $\ell \simeq \ell_{mb}$ gas. When this gas is introduced at large radii ($r \simeq 100$ M) it cannot support itself in a Keplerian orbit, as gas in the standard thin disk model can. Such an inflow thus represents the generalization of the Bondi spherically symmetric accretion problem (see refs. in Paper I) to the case of low angular momentum accretion. The gas must spiral in dynamically until it reaches the orbit appropriate to its angular momentum. We pose the question: can this cold gas then settle into some form of thin or thick disk while obeying the laws of hydrodynamics? If so, what are the generic properties of such disks?

A second goal is to study the possible flow patterns at the inner regions of disks. Pressure supported thick disks are believed to have nearly constant specific angular momentum along their inner edges, an angular momentum low enough to allow for inflow into the hole over the potential cusp (i.e., through a hole in the funnel wall). This inflow scenario was first suggested by B. Paczyński (unpublished) and has been discussed in detail[19]. Our investigation will shed light on the hydrodynamic properties

of such nonviscous inflows. Furthermore, in the standard analytic thin disk model[29], one assumes no further heating as the gas dynamically spirals into the hole from the last stable circular orbit at r = 6 M. We investigate this assumption using the equations of hydrodynamics.

The infalling gas might already be hot (ε = binding energy) at r = 100 M. We have investigated some of these models as well. However, for the purposes of comparing the flow behaviors of different accretion scenarios, we will assume the gas is initially cold and restrict the discussion in this paper to only two parameters: 1) the initial geometric thickness of the inflow, and 2) the value of ℓ. Our models further assume that all the gas has the same values of (ℓ, U_t) as it enters the grid at r = 100 M. Other inflow boundary conditions can and have been studied with our code[10].

We will describe four archetypical models which we believe delineate qualitatively different features in this two parameter space. In order, we will examine: 1) thick inflow with $\ell > \ell_{mb}$, 2) thin inflow with $\ell > \ell_{mb}$, 3) thin inflow with $\ell_{ms} < \ell < \ell_{mb}$, and 4) thick inflow with $\ell_{ms} < \ell < \ell_{mb}$. Thick and thin inflow with $\ell < \ell_{ms}$ is discussed briefly. Table I summarizes our mapping out of the solution phenomenology of this parameter space.

Table I Flow Regimes For Black Hole Accretion

Angular Momentum	Thin Inflow	Thick Inflow
$\ell < \ell_{ms}$	All Gas Flows Into Hole On Dynamical Timescale	
$\ell_{ms} < \ell < \ell_{mb}$	Entire Flow Into Hole Shock Heating Near Horizon Nozzle Flow Onto Hole	Thick Disk Forms Some Funnel Outflow
$\ell > \ell_{mb}$	Two Temperature Disk Forms Hot Wind Outflow No Flow Into Hole	Thick Disk Forms Large Funnel Outflow No Flow Into Hole

THICK DISK FORMATION AND HOLLOW JETS

First consider an accretion problem with a geometrically thick inflow with angular momentum $\ell > \ell_{mb}$. The cold ($\varepsilon = 10^{-5}$, h = 1.0) uniform density fluid is continually sent onto the grid at the outer boundary (r = 100 M) at every point up to the funnel wall defined by its angular momentum (ℓ = 4.5 M > ℓ_{mb}) and energy (U_t = -1.0). Inflow occurs with a radial freefall velocity. The outer boundary condition for this model has been modified by allowing the inflow velocity to vary to permit outflow at the boundary if the hydrodynamical solution requires it. If no

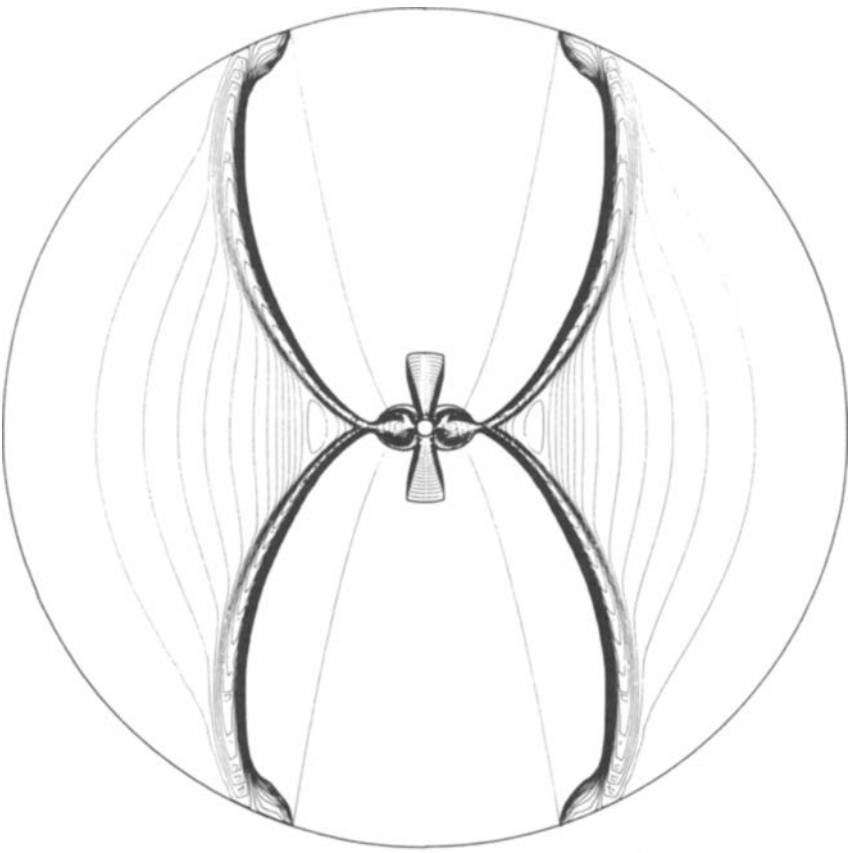


Fig. 4. The ℓ = 4.5 M thick inflow run at t = 500 M, roughly one freefall time from the outer boundary of r = 100 M. The funnel wall is shown with a single dark line. The heavy convergence of dark lines is the rapid falloff of density at the edge of the infalling fluid. Just outside this is the standoff shock. The last remnants of the initial Bondi accretion fluid is draining into the north and south poles of the black hole. The calculation resolution is 160 zones in θ from 0 to π, and 160 zones in r, staggered logarithmically, from 2 M to 100 M.

outflow occurs, steady inflow continues throughout the calculation. The initial condition is created by placing a Bondi, zero angular momentum solution (spherically symmetric) on the grid and matching the density and pressure to those of the incoming fluid at the outer boundary. This fluid will smoothly fall into the hole ahead of the high-ℓ gas coming from the boundary, lessening the transients which would be associated with fluid pouring onto a vacuum grid.

The funnel wall appropriate to this hU_t and ℓ is the outer line in Figure 3. It is clear that all the fluid will hit a

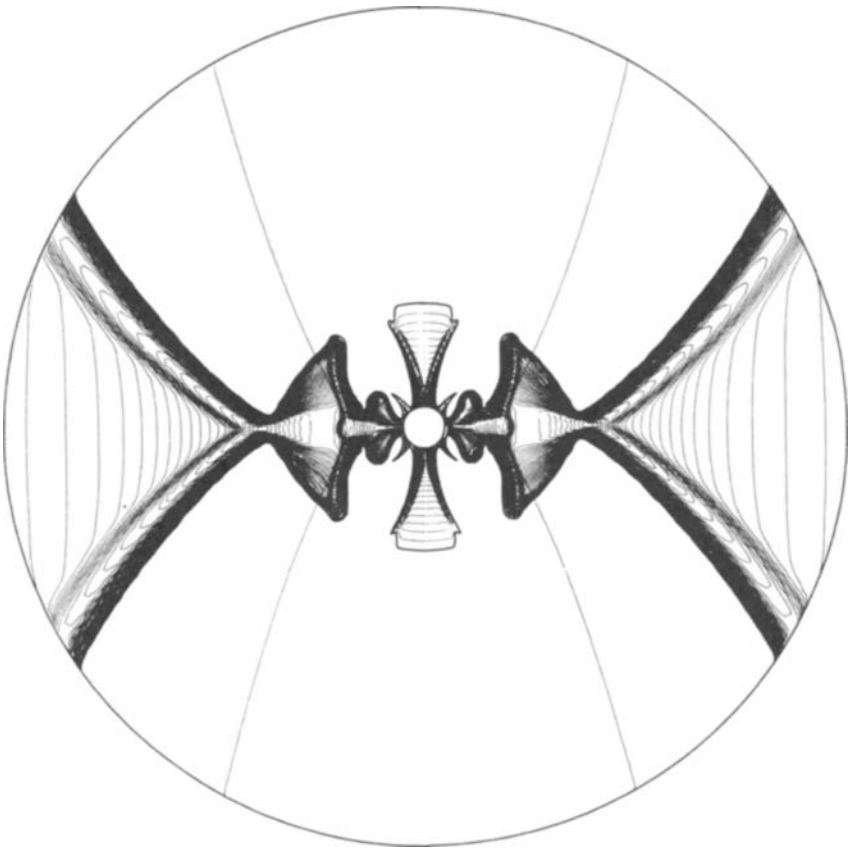


Fig. 5a. Same run as Figure 4 but at t = 570 M. This is a closeup with the outer edge at r = 30 M.

wall, a hydrodynamic fluid shocks. It is perhaps misleading to say that the fluid shocks at the funnel wall; it is the centrifugal deceleration (increasing towards the wall) which causes the shock. Nevertheless, the idea of a shock at a wall is a useful working analogy.

To understand the dynamic nature of the funnel region in this hydrodynamic accretion flow, it is useful to look in some detail of fluid density. The contour spacing is such that the fluid density doubles with every four contour levels. The first of these figures is Figure 4, at one freefall time from the outer boundary (t = 500 M). It shows that even though the fluid is first sent onto the grid radially at every point from the equator up to the static funnel wall, the flow does not remain radial. As the high angular momentum supersonic flow begins to feel the centrifugal deceleration, funnel wall standoff shocks form. These standoff shocks turn the flow sharply towards the equator; the

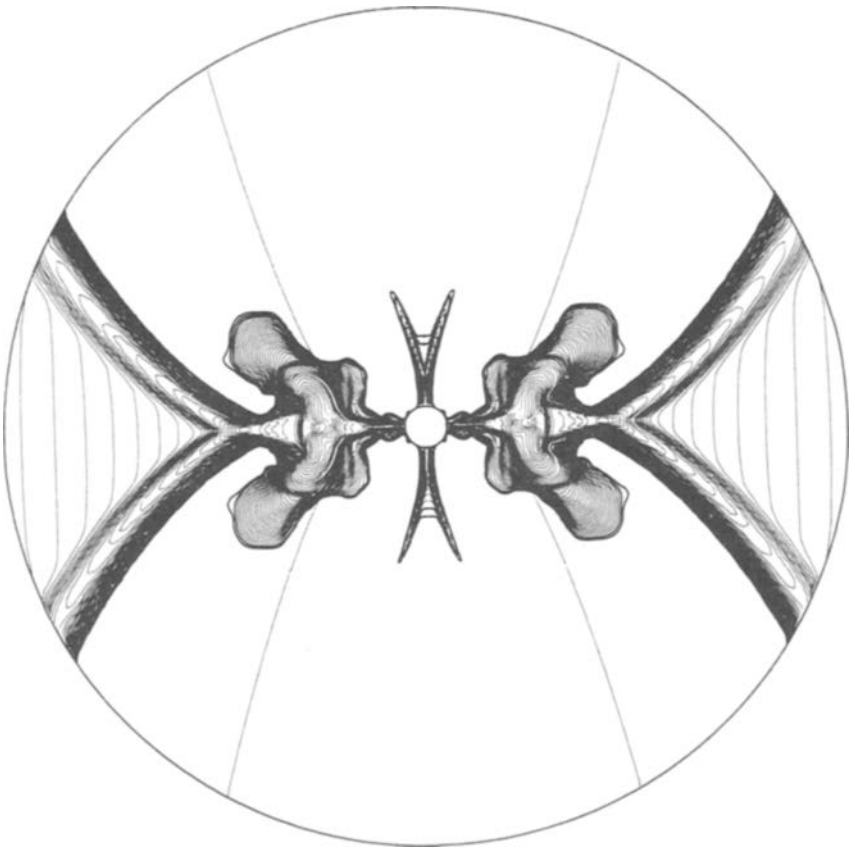


Fig. 5b. Same run as Figure 4 but at t = 620 M. This is a closeup with the outer edge at r = 30 M.

shocked fluid then flows down along the inside of the shock surface. In Figure 4, the heavy black curve lines represent the surface of the inflow while the closely spaced contour lines slightly outside of that surface represent the shock. Note that there is a large region of vacuum between the surface of the fluid and the static funnel wall (thin black line). This vacuum is centrifugally supported by the rotation of the fluid. This region will later act as the "escape route" for the shock heated gas. Note that as a leftover from our Bondi initial conditions, the last remnants of the zero angular momentum fluid inside the funnel wall can be seen falling into the north and south poles of the black hole.

The high-ℓ shocked fluid flows toward a point on the equator where the funnel wall standoff shocks cross. This crossing point occurs at r = 16 M which is very close to the circular orbit appropriate to this specific angular momentum. After all the

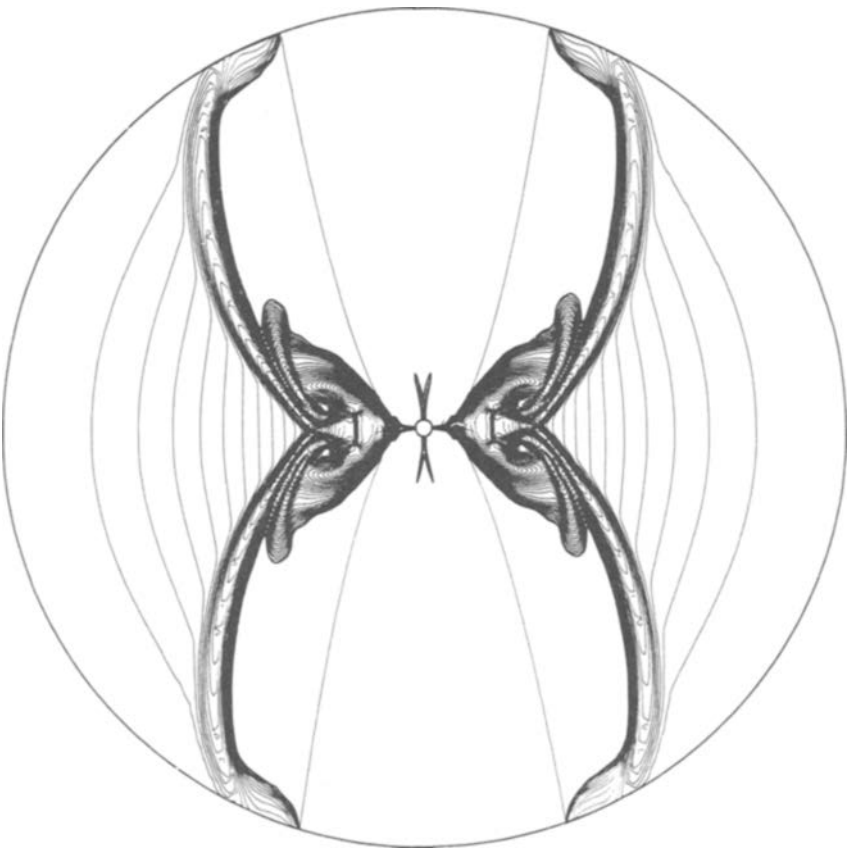


Fig. 6. Same run as Figure 4 but at t = 775 M. Outer edge is at r = 100 M.

heated fluid (now with $\varepsilon \simeq 0.01$) converges into the equatorial plane, it expands as it accelerates toward the hole.

At the end of the expanding equatorial stream, the fluid is centrifugally decelerated at the centrifugal barrier. In Figure 4 (t = 500 M), the enormous impulsive pressure gradient forces have temporarilly overwhelmed the centrifugal deceleration and are forcing some fluid through the funnel wall and into the hole. Two closely spaced stages of the rebound which follow are shown in closeup in Figure 5 (at times: a] t = 570 M and b] t = 620 M). In Figure 5a, one can see a strong shock forming near the funnel wall, as well as another pair of shocks forming even closer to the hole. We find that despite the close proximity of the flow to the horizon itself, these shocks nonetheless propagate upstream away from the hole. Although a small amount of material is forced through the funnel wall and into the hole by the high pressure gradients, most of the shocked gas rebounds backward from the

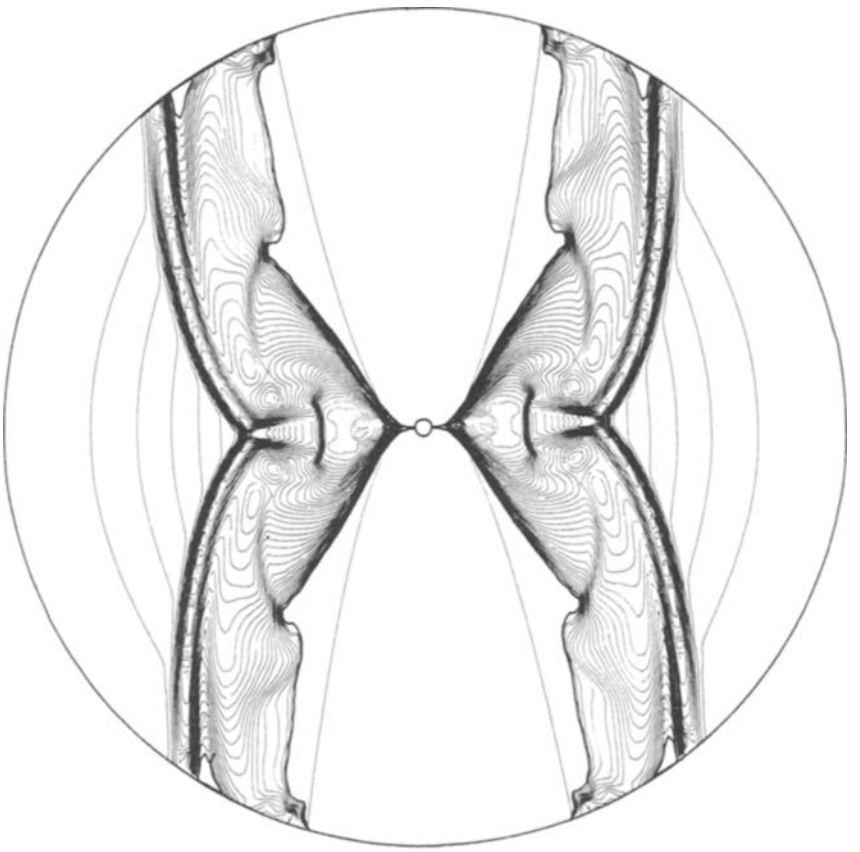


Fig. 7. Same run as Figure 4 but at t = 1300 M. Outer edge is at r = 100 M.

hole. As the shock formed off the funnel wall moves backwards, its central region becomes a "Mach ring", i.e., an accretion shock front perpendicular to the equator. Hereafter, we refer to this backward moving shock as the "accretion shock." Another example of such near hole shocks has previously been discussed[9] and illustrated in detail in Figures 3-5 of that paper.

The black hole accretion shock acts much like an accretion shock in a neutron star or white dwarf accretion flow which brings the supersonic flow to subsonic velocities. There is, of course, no solid surface for a black hole such as exists on a neutron star or white dwarf; however, our calculations demonstrate that the centrifugal barrier can, for all practical purposes, act like a solid surface off of which the fluid can shock. This is the most important aspect of black hole inflows with angular momentum which our computer runs have uncovered. Even a relatively low value of ℓ can create an effective surface for the black hole.

The hot, subsonic post-shock fluid then begins (Fig. 5b, t = 720 M) to splash back from the centrifugal barrier into the vacuum region evacuated by the previously formed funnel wall standoff shocks. By time t = 775 M (Fig. 6) this backflow has run into the infalling fluid and the "backflow standoff shock" forms to divert the flow away from the equator and up along the interior of the surface of the inflowing fluid. This processed fluid is now freely flowing up along the channel between the funnel standoff shocks and the static funnel wall. Much later at t = 1300 M (Fig. 7; note the last three figures, 5a, 5b, and 6 were separated by only 50 M in time), the full flow pattern has been established.

The thick inflow shock structures are schematically illustrated in Figure 8. To quantify the Figure, we follow the thermal history of an infalling gas cell through this shock

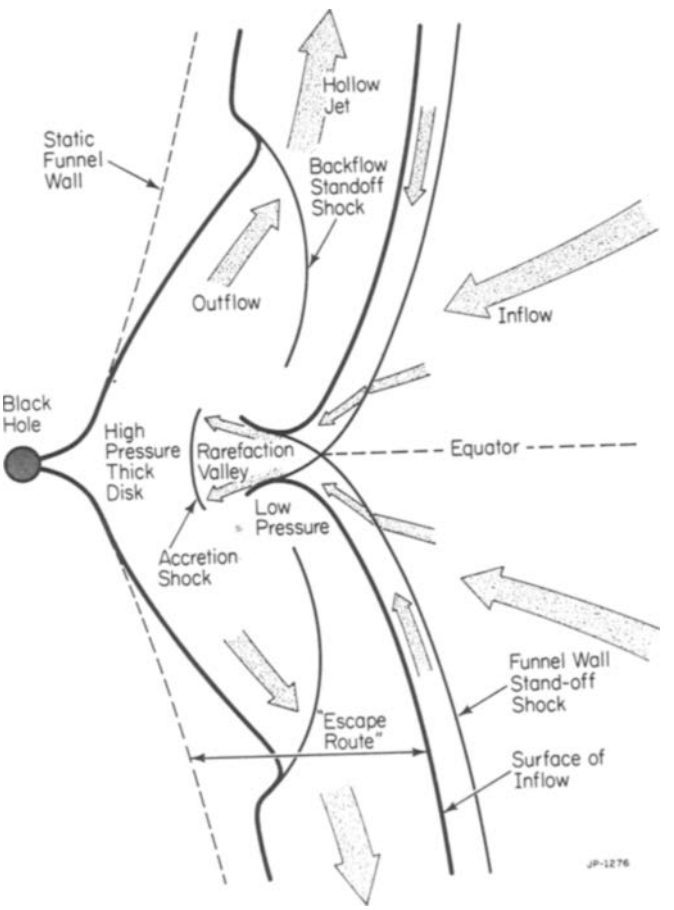


Fig. 8: Schematic diagram of shock structures and flow features seen in Fig. 7. These late time structures seem generic and stable.

structure. It begins at the outer boundary with $\varepsilon = 10^{-5}$ and $U_t = -1.0$. On the fall from the outer boundary, adiabatic heating increases the temperature of the fluid by 50% prior to the first shock heating. The standoff funnel shocks raise the temperature to an average of 0.007 (the temperature and shock strength decrease as the height above the equator increases). The standoff shocks do not bring the gas to rest, rather it accelerates through the rarefaction valley until it hits the accretion shock. There its radial motion is stopped, forming a thick pressure supported disk.

The reason that the accretion shock was able to stop the gas can be understood in terms of the energy of the circular orbit and the shock strength. In order for the shock to bring the fluid to rest, it must convert all the kinetic energy to internal energy, i.e., it must lower the fluid's energy $-U_t$ from 1.00 to the value associated with the circular orbit. Since $hU_t = (1 + 4\varepsilon/3)\, U_t$ is conserved in the shock, this means that the temperature ε must be raised accordingly. For fluid with a specific angular momentum of $\ell = 4.5$ M, the circular orbit is located at r = 15.3 M, with an energy $-U_t$ of 0.970. This requires that ε to rise to 0.023. We find in our model that the pressure maximum of the disk is actually located at r = 15 M with an $\varepsilon = 0.02$, and an energy $-U_t = 0.970$, in very close accord with our analytic expectations. It should be noted that these results are consistent with a numerical error in the energy of about 5%.

The high pressure of the hot disk drives shocked fluid into the lower pressure "escape route" between the standoff funnel shocks and the static funnel wall (see Figs. 5b, 6, 7). It is once again shocked by the "backflow standoff shock" which diverts the outflow and prevents it from colliding with the infalling fluid. A portion of the outflowing fluid finally leaves the outer grid with $\varepsilon = 0.01$ and $-U_t = 0.987$ (still slightly bound). Many of the shock features and flow patterns shown in Figure 8 also occur in the propagation of supersonic jets in the Newtonian nongravitational regime[30-35].

This $\ell = 4.5$ M model demonstrates that hot, pressure supported thick disks can be formed as a natural part of the hydrodynamic structures of accretion flows with angular momentum $\ell > \ell_{mb}$. However, the disk which is formed is not the stationary structure envisioned by the analytic disk theory. The disk is but a density enhanced pattern in a complicated inflow and outflow. Further, when dynamic infall plays a role in disk structure or formation, the disk cannot be isentropic. To bring fluid to rest requires a backwards traveling shock, a shock which will decrease in strength as it climbs out of the potential. Thus, the jump in entropy of the gas forming the thick disk will decrease with time.

We further conclude that while this accretion scenario is effective in shock heating fluid and driving an outflow, it does not produce a collimated outflow. Nothing has reduced the specific angular momentum in the fluid and the U_ϕ term in the Euler equation remains important. The flow seeks to move away from the orbital axis to the extent that it is permitted. In this

thick flow, this means up along the funnel wall. Thus, these hydrodynamic processes form hollow conical jets. The same angular momentum which formed a funnel in the first place guarantees that the outflow generated from this same fluid will be driven along the exterior of the funnel wall, not up the funnel interior.

It is also apparent from this run that purely hydrodynamic process do not produce highly energetic outflows. The hollow jets do not have a total energy significantly in excess of the energy of the infalling fluid. Nonetheless, this model does show one new way in which outflow of hot gas from near the hole can occur. But clearly, an acceleration mechanism other than hydrodynamic shocks is required to produce the observed highly energetic jets. Further, if there is to be near hole collimation, then the angular momentum which makes these jets hollow must be contended with whenever the disk supplies the jetted material.

An interesting facet of these hollow jets is that they effectively line the funnel walls with hot material. The funnel is, by definition, an evacuated column extending out away from the hole. The funnel can therefore serve as a channel through which radiation emitted by the hot outflow escapes to infinity. The hydrodynamic process has produced hot gas and placed it in such a position as to allow it to effectively radiate into the vacuum funnel interior. Whether this new picture of a black hole accretion flow can overcome the objections for radiation driven jets, metioned above, remains to be seen.

TWO TEMPERATURE DISK WITH HOT WIND

We now consider the identical startup parameters, except that the width of the inflow is narrow and the fluid enters the outer boundary as a thin ring. The fluid freefalls until it encounters the centrifugal deceleration near the funnel wall. An accretion shock forms which heats the fluid to a temperature of $\varepsilon \approx 0.002$, but not high enough to bring the fluid to rest. The hot, shocked fluid can no longer be confined to the equatorial plane; it flows outward, above and below the thin disk in a hot wind.

An intermediate stage in the process is depicted in Figure 9 at $t = 1650$ M after the start of the infall (again the freefall time is about 500 M). As before, the contours represent the logarithm of density. The inflowing fluid is the wedge along the equator. The accretion shock is nestled into the funnel wall and the flow emerging from this shock surface moves up and back around the inflow. Note that there are no standoff funnel wall shocks because the fluid encounters the funnel wall only in the equatorial plane. As more and more fluid is processed through the accretion shock, the thickness of the disk increases and a vertical pressure gradient develops. A fully dynamic two temperature disk forms with heat provided by the shock. Such a disk does not resemble the traditional equilibrium thick disk[36]. It is instead a two temperature structure with cool (pre-shock) gas inflowing along the equator and a surrounding wind of hot (post-shock) gas flowing out.

In contrast to the thick inflow, the resulting outflow looks less like a hollow jet and more like a hot wind. Because the heated fluid is not confined by an inflow along the funnel standoff shocks as in the previous case, it is free to flow almost radially outwards, surrounding the inflow. Eventually, it provides sufficient pressure above and below the inflow, to confine the inflow in an equatorial stream. The lack of geometric confinement and insufficient accretion shock strength causes a standing shock to form rather than the slowly outward traveling accretion shock.

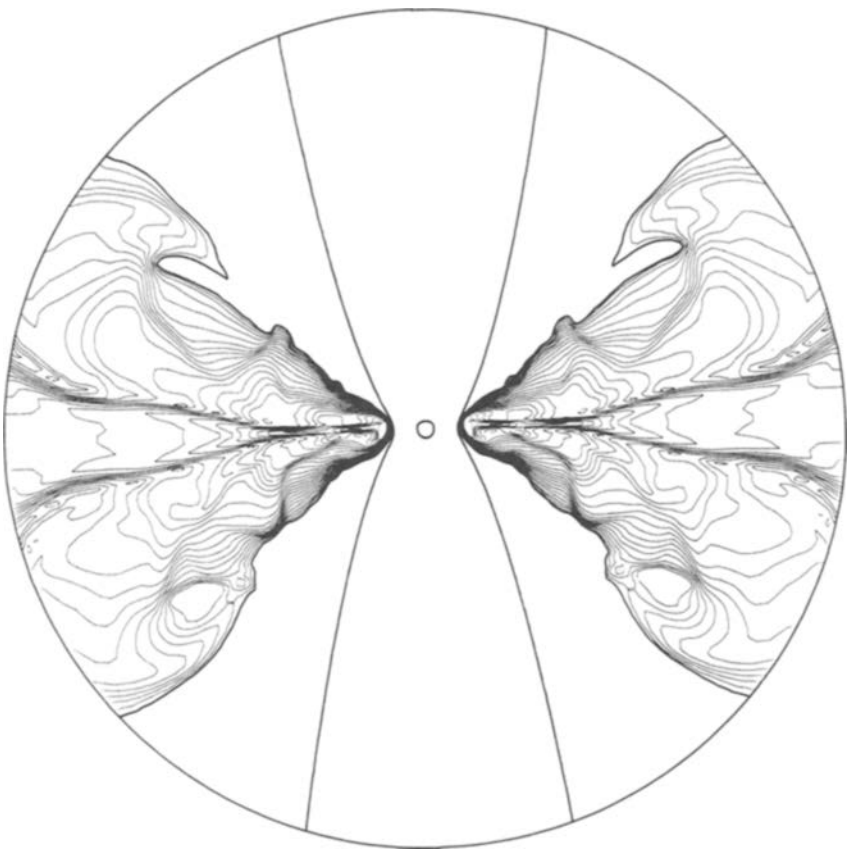


Fig. 9. The ℓ = 4.5 M thin inflow at t = 1650 M. The wedge of material in the equatorial plane is the inflowing gas, the wind above the disk has been shock heated at the accretion shock just outside the funnel wall. Note that there is no funnel wall standoff shock as there is in Figure 7. For this value of ℓ, no flow goes down the hole.

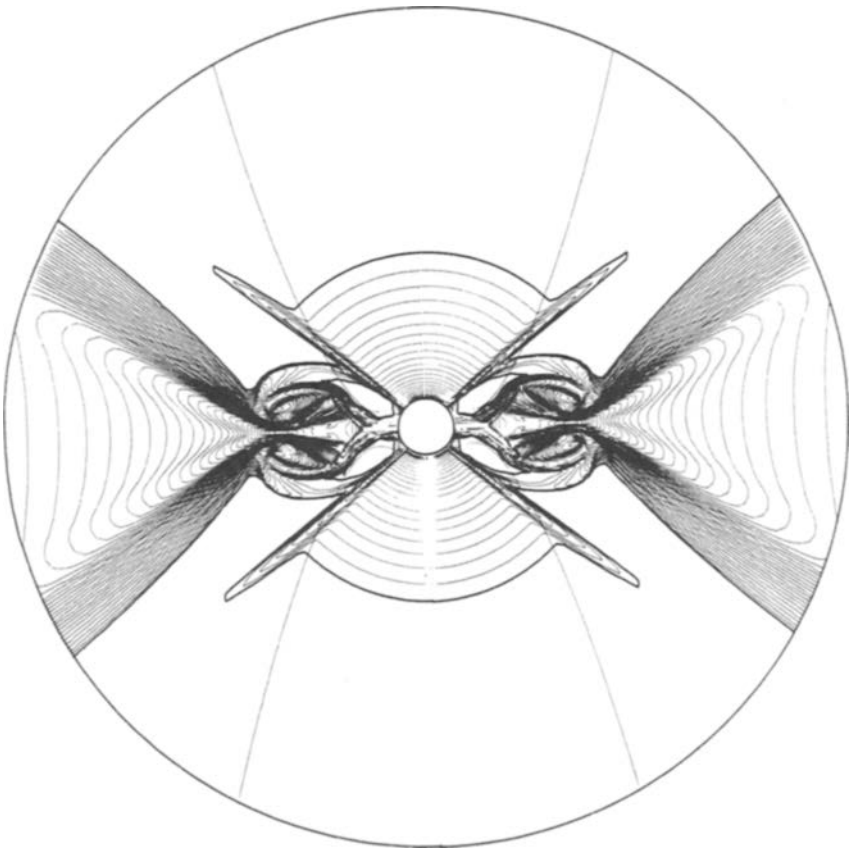


Fig. 10. The ℓ = 3.8 M thin inflow at t = 970 M in closeup (outer edge r = 30 M). Note that the funnel wall does not intersect the equator. Even so, the fluid shocks off the overhanging funnel wall. The flow cannot be reversed by the centrifugal acceleration and the entire flow is focused down the hole.

LIFE INSIDE 6M - NOZZLE ACCRETION INTO HOLES

We now consider what happens when we rerun the thick and thin inflows, but with a slightly lower specific angular momentum than the ℓ = 4.5 M used in the model described above. We will use a value of ℓ = 3.8 M which is below the marginally bound value of $\ell = \ell_{mb} = 4.0$ M while staying above the marginally stable value of $\ell = \ell_{ms} = 3.46$ M. As seen in Figure 3, the funnel wall is now open onto the hole and inflow into the hole becomes possible.

The first run with ℓ = 3.8 M has the same thin inflow outer boundary condition as that of the ℓ = 4.5 M run shown in Figure 9.

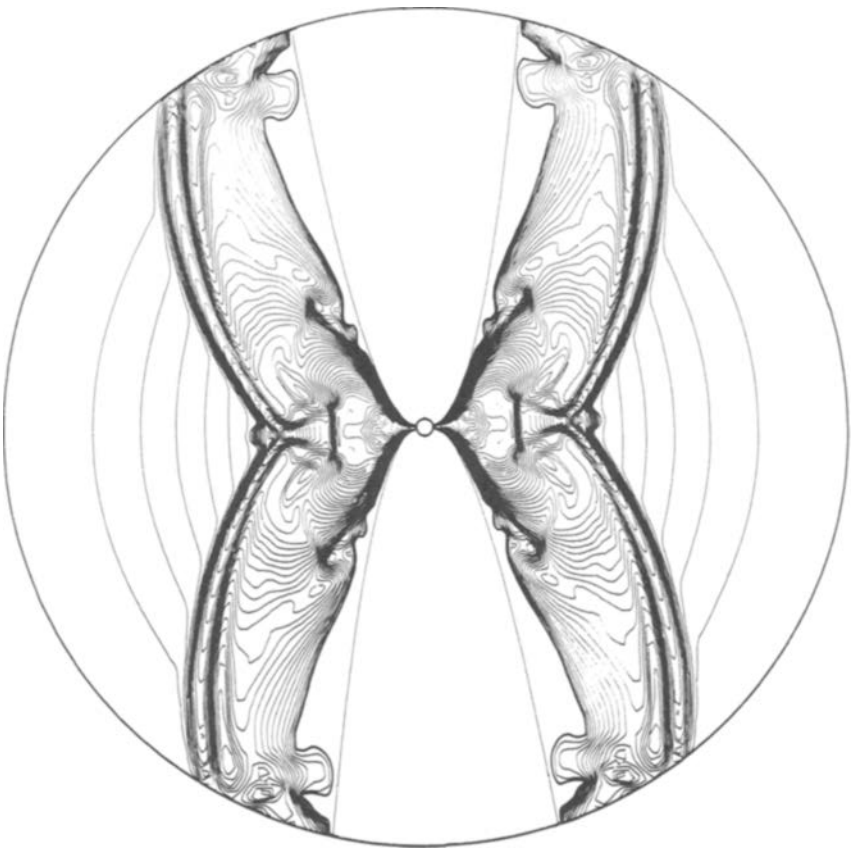


Fig. 11a. The ℓ = 3.8 M thick inflow at t = 1700 M. Compare to Figure 7 to see the great similarity.

However, as shown in Figure 10, the ℓ = 3.8 M flow is completely different. Such a fluid has a centrifugal barrier which turns over at r = 4.57 M (see Figure 2). To hit this barrier, the fluid's energy must drop below $-U_t$ = 0.959. As Figure 10 shows, the inflow proceeds smoothly from the outer boundary to a convergence point on the equator. Here an equatorial stream forms, similar to the ones noted in the ℓ = 4.5 M run above. A pair of criss-cross shocks form at r = 10 M where $-U_t$ is reduced to its minimum value of 0.987. Note that this is insufficient to permit the fluid to hit the centrifugal barrier. Interior to this point, the flow expands in a rarefaction valley. However, there is no terminal accretion shock to further reduce the energy $-U_t$ and therefore the flow continues, unhindered, into the hole. No thick disk, no hot wind, and no hollow jet is created.

In contrast, we now consider the effects of reducing ℓ below the marginally bound value when the flow is geometrically

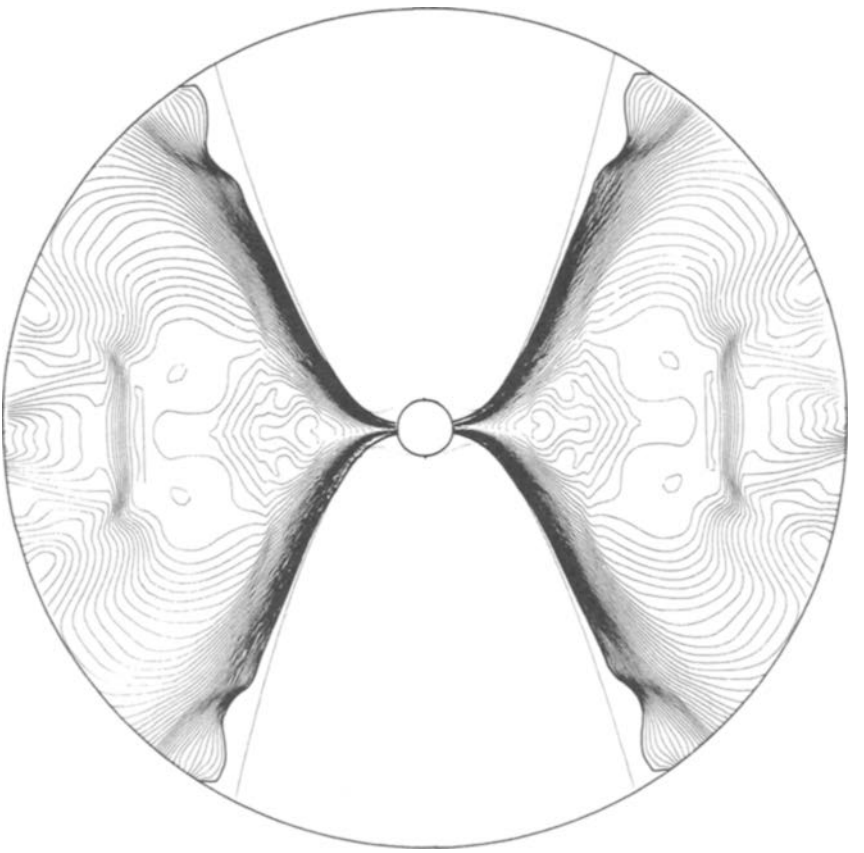


Fig. 11b. A closeup of Figure 11a with outer edge r = 30 M. Note that the funnel wall focus the flow into the hole through a "nozzle." About 4% of the inflow from r = 100 M goes down the hole.

thick. We will use the same thick inflow boundary conditions as in the ℓ = 4.5 M run shown in Figures 4-8, but with the lower ℓ = 3.8 M value for the specific angular momentum used in Figure 10. The formation of the funnel wall standoff shock and the rarefaction valley proceed as in the high angular momentum (ℓ = 4.5 M) thick inflow case described above. This is illustrated at time t = 1700 M in Figure 11a. Because of the greater convergence of fluid to the equator, the criss-cross shocks in the thick run are stronger than those in the thin inflow (Figure 10) by a factor of 10, as measured by pressure jump. In spite of this, it is still not strong enough to reduce $-U_t$ below the critical value. However, the enhanced pressure in the rarefaction valley pushes the fluid away from the equator and up against the overhanging funnel wall, increasing the centrifugal

deceleration which in turn creates an accretion shock, allowing formation of a thick, hot disk. As in the ℓ = 4.5 M run (Figure 7), we see that the thickness of the inflow leads to drastically different accretion structures even though the angular momentum of the fluid is the same in Figures 10 and 11a.

Let us compare in more detail the two thick inflow runs of different angular momenta, represented by Figures 11 and 7. The single most important change is that inflow into the hole, proscribed in the ℓ = 4.5 M case, is now possible. A new feature, which we refer to as the "nozzle", forms at the inner edge of the disk. Here, an inward pointing pressure gradient drives inflow through the opening in the funnel wall and into the hole. A closeup of the fat disk and accretion nozzle is given in Figure 11b.

What are the characteristics of the flow through this nozzle? Inside of the accretion shock, the fluid velocities are subsonic. However, the inflow into the hole is supersonic, hence there is a sonic point within the nozzle. The nozzle flow begins at the inner edge of the disk at a radius of r = 5.5 M and the sonic point occurs at r = 4.4 M. It is interesting to note that for U_ϕ = 3.65 M, which characterizes the fluid in the nozzle, the unstable circular orbit (local effective potential maximum) is at r = 4.56 M. Thus, the flow goes transonic inside of the potential barrier peak.

The accretion rate through the nozzle and into the hole is constant after the nozzle flow has been established. In steady state the flow into the hole is 4% the amount of fluid sent onto the grid. Clearly, much more fluid is coming onto the grid than the nozzle can handle. This suggests that the nozzle is capable of supporting only a limited inflow rate. When the accretion rate exceeds this limit, fluid piles up and a thick disk forms.

The nozzle is quite similar to a deLaval nozzle[37-39]. The nozzle walls are provided by centrifugal confinement. Given a fixed entropy, energy hU_t and a transonic point in the nozzle, the mass flux is fixed. A larger accretion rate requires that the nozzle "walls" expand, resulting in centrifugal deceleration and the shock heating required to reduce U_t below the critical value.

In addition to its role in creating shocks and promoting disk formation, the nozzle plays an important role in the static fat disk model[19,20,36] by providing the mechanism for the final accretion into the hole. In this picture, viscous stress acts to lower the fluid's angular momentum sufficiently to permit flow past the maximum in the effective potential, i.e., through the funnel wall. The transonic nozzle observed in this model is exactly the hydrodynamics expected. Our calculation shows that such an inflow nozzle arises naturally in the accretion of low angular momentum fluid ($\ell < \ell_{mb}$), and demonstrates the viability of the idea that the final inflow from a thick disk into the hole is through just such a nozzle.

Of course, the formulation of a complete fat disk model involves viscosity and many questions remain unanswered. For example, can viscous stress increase the accretion rate above what

can be handled by the nozzle? Presumably shocks would then occur driving outflow along the funnel wall in a manner analogous to that discovered in these calculations. Alternatively, viscosity along the inner edge of the disk might reduce the angular momentum sufficiently to open the nozzle up, thereby increasing the permitted inflow rate. These questions regarding what dynamics might be induced by viscosity can only be answered by a more complete model. Nevertheless, the hydrodynamic processes we have describe remain applicable in the flows which result.

CONCLUSIONS

Our aim in this paper has been to describe new hydrodynamic pheomena in black hole accretion flows and suggest alternative ways to look at the role of the funnel. First and foremost, these results are an extension of the Bondi spherical accretion problem to nonspherical inflows. But these calculations also suggest modifications to both the standard thin and fat disk paradigms.

In the Bondi solution, the angular momentum is zero; the inflow is purely radial. The fluid is adiabatically heated as it falls, but this heating is very inefficient. All the gas falls into the hole. The flow, initially subsonic at large r, passes through a transonic critical point at some radius and infalls supersonically with a velocity on the order of, but below, free fall. Since a black hole has no surface, the inflow does not end in an accretion shock; it merely passes into the hole without affecting the fluid behind it.

This scenario is qualitatively changed by even a small amount of angular momentum. Consider the canonically "insignificant" angular momentum, that less than the marginally stable value. While we did not specifically discuss this case here, we have performed a number of calculations which show that despite the lack of a stable circular orbit, even this low value of ℓ alters the inflow by creating an evacuated funnel along the orbital axis. Furthermore, standoff shocks are formed which focus the flow into the hole through the equatorial plane--a very nonspherical form of accretion. Whether there is any flow with angular momentum which resembles Bondi flow remains to be determined.

As ℓ increases to the point (ℓ_{ms}) where a stable circular orbit is possible, an orbital turning point is created (Figure 2). This centrifugal barrier begins to hinder inflow into the hole. If the fluid is marginally bound, and $\ell < \ell_{mb}$, enough kinetic energy may be retained to overcome this potential barrier. This occured in the thin inflow model (Figure 10). However, the funnel walls restrict the available space through which the fluid can flow into the hole. This creates an effective nozzle, and the fluid shocks when the inflow is greater than what the nozzle can carry. Such was the case in the thick inflow model with $\ell = 3.8$ (Figure 11). The nozzle continues to support flow into the hole at a fixed rate but, when the total inflow rate exceeds that level, fluid piles up and a hot disk forms. This

disk drives outflow through the evacuated space between the static funnel wall and the inflowing fluid's surface.

When the angular momentum is greater than marginally bound, the nozzle closes (Figure 2) and none of the infalling fluid ends in the hole. The thin inflow model changes drastically from the $\ell < \ell_{mb}$ case, where all the flow goes down the hole, to a flow which blows away from the hole in a hot wind. The thick inflow model is very similar to the $l < l_{mb}$ case, except that now no flow goes into the hole through the nozzle.

We have emphasized only those features which arise from consideration of the fluid dynamics in the near hole region, yet the fluid dynamics alone are sufficient to produce interesting and important new phenomena. Historically, the move from the standard analytic thin disk theory to the comparative complexity of the analytic thick disk was achieved simply through the addition of pressure. In our models, we take this a step further by considering time-dependent flows. In each of these cases, important and unanticipated features emerge from the addition of new physics. We anticipate that this trend will continue as additional effects, including radiation transport, viscous torques, magnetic fields, and turbulence are added in the development of a realistic, complete theory. Such a theory would tell us which effects dominante and in what circumstances. However, even when additional physical processes are considered, the richness of the hydrodynamical pheomena we have reported on herein remains to be reckoned with.

ACKNOWLEDGEMENTS

We thank the Max-Planck-Institut für Physik and Astrophysik, Institut für Astrophysik, and its Director Kippenhahn for their hospitality, generous support, and the use of the CRAY-1 computer upon which these calculations were performed. The tireless and patient help of our coworkers Karl-Heinz Winkler and Michael Norman is gratefully acknowledged. In addition we thank Martin Rees, Mitch Begelman, Roger Blandford, James Wilson, Dean Sumi and William Press for useful discussions, and Richard Brandolino for assistance with software development for the data analysis, performed on the University of Illinois Vax and Image Processing System.

REFERENCES

1. Begelman, M. C., Blandford, R. D., Rees, M. J., Rev. Mod. Phys., **56**, 255 (1984).
2. Willis, B. et. al., Astrophys. J., **274**, 62 (1983).
3. Hawley, J. F., Smarr, L. L., Wilson, J. R., Astrophys. J., **277**, 296 (1984 Paper I).
4. Hawley, J. F., Smarr, L. L., Wilson, J. R., Astrophys. J. Suppl. Ser., **55**, 211 (1984 Paper II).
5. Wilson, J. R., Astrophys. J., **173**, 431 (1972).

6. Wilson, J. R., from Ann. N. Y. Acad. Sci., **262**, 123 (1975).
7. Wilson, J. R., in Proceedings of the Marcel Grossman Meeting ed. R. Ruffini (Amsterdam: North Holland, 1977), p. 393.
8. Wilson, J. R., in Proceedings of the Int. Sch. of Phys. Fermi Course LXV, eds. R. Giacconi and R. Ruffini (Amsterdam: North Holland, 1978), p. 644.
9. Hawley, J. F., Smarr, L. L., in Problems of Collapse and Numerical Relativity, eds. D. Bancel and M. Signore (Dordrecht: Reidel, 1984), p. 253.
10. Hawley, J. F., Ph.D. Thesis, University of Illinois, (1984).
11. Zabusky, N. J., Physics Today, July 1984, p. 36.
12. Ruffini, R. and Wilson, J. R., Phys. Rev. D, **12**, 2959 (1975).
13. Damour, T., Hanni, R. S., Ruffini, R., Wilson, J. R., Phys. Rev. D, **17**, 1518 (1978).
14. Sloan, J. H. and Smarr, L. L., in Numerical Astrophysics: A Festschrift in Honor of James R. Wilson eds. J. Centrella, R. Bower, and J. LeBlanc (Boston: Jones and Bartlett, 1984), p. 52.
15. Thorne, K. S., Macdonald, D., Mon. Not. R. Astron. Soc. **198**, 339 (1982).
16. Misner, C., Thorne, K., and Wheeler, J., Gravitation (San Francisco: Freeman, 1973).
17. Smarr, L. L., Taubes, C., Wilson, J. R., from Essays in General Relativity, ed. F. J. Tipler (New York: Academic Press, 1980), p. 157.
18. Shakura, N. I., Sunyaev, R. A., Astron. Astrophys. **24**, 337 (1973).
19. Kozłowski, M., Jaroszynski, M., Abramowicz, M. A., Astron. Astrophys. **63**, 209 (1978).
20. Abramowicz, M. A., Jaroszynski, M., and Sikora, M., Astron. Astrophys., **63**, 221 (1978).
21. Abramowicz, M. A., Acta Astron., **24**, 45 (1974).
22. Fishbone, L. G., Moncrief, V., Astrophys. J., **207**, 926 (1976).
23. Lynden-Bell, D., Phys. Scripta, **17**, 185 (1978).
24. Abramowicz, M. A., Piran, T., Astrophys. J. Lett., **241**, L7 (1980).
25. Sikora, M., Wilson, D. B., Mon. Not. R. Astron. Soc. **197**, 529 (1981).
26. Nobili, L., Turolla, R., Calvani, M., Lett. Nuovo Cimento, **35**, 335 (1982).
27. Piran, T., Astrophys. J. Lett., **257**, L23 (1982).
28. Rees, M. J., Begelman, M. C., Blandford, R. D., Phinney, E. S., Nature, **295**, 17 (1982).
29. Novikov, I., Thorne, K. S., in Black Holes, ed. B. DeWitt and C. DeWitt, (New York: Gordon and Breach, 1973), p. 343.
30. Norman, M. L., Smarr, L. L., Winkler, K.-H. A., Smith, M. D., Astro. Astrophys., **113**, 285 (1982).
31. Norman, M. L., Winkler, K.-H. A., Smarr, L. L., in Astrophysical Jets, ed. A. Ferrari, A.G. Pachokzyk (Reidel: Boston, 1983), p. 227.

32. Norman, M. L., Smarr, L. L., Winkler, K.-H. A., in Numerical Astrophysics: A Festschrift in Honor of James R. Wilson, ed. J. Centrella, R. Bowers, and J. LeBlanc (Boston: Jones and Bartlett, 1985), p. 88.
33. Smarr, L. L., Norman, M. L., Winkler, K.-H.A., Physica 12, 83 (1984).
34. Smith, M. D., Norman, M. L., Smarr, L. L., Winkler, K.-H.A., Mon. Not Roy. Astron. Soc., submitted (1984).
35. Norman, M. L., Winkler, K.-H. A. in Astrophysical Radiation Hydrodynamics ed. K.-H.A. Winkler and M. L. Norman (Reidel: Boston, 1985), in press.
36. Abramowicz, M. A., Calvani, M., Nobili, L., Astrophys. J., 242, 772 (1980).
37. Courant, R. and Friedrichs, K. O., Supersonic Flows and Shockwaves, (New York: Springer Verlag, 1948).
38. Norman, M. L., Smarr, L., Wilson, J. R., and Smith, M. D., Astrophys. J., 247, 52 (1981).
39. Smith, M. D., Norman, M. L., Smarr, L. L., Wilson, J. R., Astrophys. J., 264, 432 (1983).